THE ASTROPHYSICAL JOURNAL, 470:L31–L34, 1996 October 10


# HELICAL STRANDS IN THE JETLIKE NARROW-LINE REGION OF ESO 428-G14

HEINO FALCKE AND ANDREW S. WILSON[1]
Astronomy Department, University of Maryland, College Park, MD 20742-2421; hfalcke@astro.umd.edu, wilson@astro.umd.edu
CHRIS SIMPSON
Space Telescope Science Institute, 3700 San Martin Drive, Baltimore, MD 21218; simpson@stsci.edu
AND
GARY A. BOWER[2]
Department of Physics and Astronomy, Johns Hopkins University, Baltimore, MD 21218; bower@pha.jhu.edu
*Received 1996 June 10; accepted 1996 August 2*

## ABSTRACT

We present *HST*/WFPC2 images of the narrow-line region (NLR) of the Seyfert 2 galaxy ESO 428-G14 (0714−2914, M4-1). The NLR consists of many individual, thin strands, which are very closely related to the radio jet and produce a highly complex, yet ordered, structure. We find that the jet is two-sided, with a double helix of emission-line gas apparently wrapped around the northwest side. To the southeast, the jet seems to be deflected at a ridge of highly excited gas. The strands to the southeast may also wrap around the radio jet, but here complete helices are not seen. The overall structure is reminiscent of the jet seen in NGC 4258. Faint symmetric features aligned with the nucleus could indicate the presence of a highly collimated beam of photons or plasma from the center.

*Subject headings:* galaxies: active — galaxies: individual (ESO 428-G14) — galaxies: jets — galaxies: nuclei — galaxies: Seyfert — radio continuum: galaxies

## 1. INTRODUCTION

The defining features of Seyfert galaxies are their narrow, high-excitation, nuclear emission lines, which indicate the presence of nonstellar, nuclear activity. The shape and size of the narrow-line region (NLR) are therefore important factors for our understanding of the processes in Seyfert galaxies in particular and active galactic nuclei (AGNs) in general. Observations of the extended narrow-line region (ENLR) have shown that this region is often elongated, and excitation maps (i.e., [O III]/H$\alpha$ ratio maps) sometimes show a sharp, straight-edged conical structure (e.g., Pogge 1988). This is well explained within the unified scheme (see Antonucci 1993), in which shadowing by an obscuring torus produces an anisotropic radiation field that excites the ambient medium.

The fact that most NLRs do not show a clear conical structure in total emission-line maps alone and that these images reveal much fine-scale structure indicate that other factors, in addition to anisotropy in ionizing radiation, affect the morphology of the NLR and the clouds therein. Neither outflow nor pure rotation seems to provide a complete description of the kinematics of the NLR clouds (e.g. in NGC 4151; Boksenberg et al. 1995), which leaves unanswered the important question of what produces and shapes the NLR.

Since the early Very Large Array (VLA) surveys of Seyfert galaxies (Ulvestad & Wilson 1989 and references therein) it has been known that a substantial fraction of Seyfert galaxies show radio jets or lobes, and many others have radio cores that may just be unresolved radio jets. Moreover, in Seyfert galaxies (de Bruyn & Wilson 1978), radio galaxies (Rawlings et al. 1989), and quasars (Baum & Heckman 1989; Falcke, Malkan, & Biermann 1995) the emission-line and radio luminosities are correlated. Further, the radio structure and the (E) NLR are closely aligned in Seyfert galaxies (Unger et al. 1987; Haniff, Wilson, & Ward 1988). Thus, the physical processes which define the relationship between radio synchrotron and thermal gases are of considerable interest.

*Hubble Space Telescope* (*HST*) observations of Seyfert galaxies (e.g., Mulchaey et al. 1994; Bower et al. 1994; Boksenberg et al. 1995; Capetti et al. 1996) show that the radio emission and the NLR are indeed closely associated. In this paper, we present *HST*/WFPC2 images of the Seyfert 2 galaxy ESO 428-G14 that shed further light on this association and especially on the interaction between the jet and the NLR.

ESO 428-G14 (0714−2914, MCG−05-18-002) was initially classified as a planetary nebula (M4-1), but Bergvall, Johansson, & Olofsson (1986) showed that it is a typical Seyfert 2 galaxy. The host galaxy is classified as SA0+. On high-resolution VLA maps, the galaxy shows an apparently one-sided, bent radio jet (Ulvestad & Wilson 1989), and Wilson & Baldwin (1989, hereafter WB89) found that the ionized gas, as imaged in [O III] and H$\alpha$ + [N II], of ESO 428-G14 is elongated in the direction of the radio jet. The [O III] emission lines have extended red wings in the northwest and blue wings to the southeast. The heliocentric redshift is $z = 0.00544$, and $1''$ corresponds to 92 pc for a Hubble constant of $H_0 = 75$ km s$^{-1}$ Mpc$^{-1}$ using the Galactic Standard of Rest velocity from de Vaucouleurs et al. (1992).

## 2. OBSERVATIONS AND DATA REDUCTION

### 2.1. *Observations*

ESO 428-G14 was observed with the Wide Field and Planetary Camera 2 (WFPC2) on board the *HST*. The filters were chosen such that they included the redshifted H$\alpha$ ($\lambda$6563) and [O III] ($\lambda$5007) emission lines and their adjacent continua, all exposures being split into two integrations, to allow cosmic-ray rejection.

[1] Adjunct Astronomer, Space Telescope Science Institute.
[2] Current address: National Optical Astronomy Observatories, P.O. Box 26732, Tucson, AZ 85726.

The Hα emission line of ESO 428-G14 is redshifted into the [N II] filter (F658N) of the WFPC2, and so we were able to use the PC chip which has a pixel scale of 0.″0455 pixel$^{-1}$. Using the spectrum from Bergvall et al. (1986) of ESO 428-G14 and the bandpass of the F658N filter, one finds that [N II] (mostly the 6548 Å line) contributes ≃33% of the emission-line flux in this image. For simplicity we will refer to our F658N images as "Hα images" despite the [N II] contribution, and no correction was applied for the [N II] contamination, as the spatial variation of the [N II]/Hα ratio is unknown. For the continuum a red broadband filter (F814W) was chosen, in which little contamination from emission lines is expected. The observations were performed on 1995 April 17, and had total exposure times of 800 and 200 s in the F658N and F814W filters, respectively.

For the [O III] image, the linear ramp filters (LRFs) and the Wide Field Camera (WFC) chips with a pixel scale of 0.″1 pixel$^{-1}$ were used. The LRFs have position-dependent peak-transmission wavelengths and FWHM bandpasses of ∼1.3%, and so they are ideally suited for redshifted emission-line objects that are less than 14″ across. The filter used for the redshifted [O III] image was FR533N, with the galaxy centered at position (675, 227) on the WF4 chip, which corresponds to a central wavelength of 5033 Å. The off-band continuum image was taken on the WF3 chip centered at position (221, 565), which corresponds to a central wavelength of 5284 Å. Those observations were performed on 1996 January 14 with total exposure times of 280 s each.

### 2.2. *Data Reduction*

All images were processed through the WFPC2 pipeline at the Space Telescope Science Institute. Flat fields are not yet available for the LRFs, so we used a flat field taken in a nearby narrowband filter (F502N). Each pair of images was combined using the IRAF task CRREJ to remove cosmic rays, and photometric calibration was performed using the WFPC2 exposure-time calculator. All images were rotated to the cardinal orientation.

Combining the LRF images taken at different positions on the WFPC requires correction for geometric distortions, and this was achieved using the IRAF task WMOSAIC. Each pair of line and continuum images was aligned using the internal astrometry of the *HST*, i.e., using the coordinate information in the image headers. Since each of the on- and off-band pairs was taken consecutively using the same set of guide stars, the relative astrometry should be excellent. The positions of three stars visible on the red on- and off-band images were found to agree to better than 20 mas.

It was then necessary to align the PC (red) and LRF (green) images. This was done by aligning the continuum peaks, which are well defined in our images, and the corresponding on-band images were shifted accordingly. Because we did not have any stars common to both images, we checked the registration by comparing the very similar morphology in the two on-band images. The good agreement indicates that the optical continuum positions (see crosses in Figs. 1*a* and 1*b* [Pl. L5]) in the two images relative to each other is not severely altered by reddening. To obtain an excitation map, the [O III] image was interpolated to match the sampling of the Hα image. Then the two images were smoothed with a beam of 0.″1 and divided by each other. The resulting map was similar to that obtained by reducing the PC image to the resolution of the WF image prior to the division.

## 3. RESULTS

### 3.1. *HST Images*

Our final images are shown in Figure 1, which reveals that the narrow-line region of ESO 428-G14 is very asymmetric, is highly elongated, and has very prominent, bright strands along its major axis. As commonly found for Seyfert 2 galaxies observed with *HST* (e.g., Wilson et al. 1993; Bower et al. 1994), the nucleus of the galaxy (taken here to be the peak of the red continuum light) is not particularly bright in emission lines. One of the most interesting features of the emission-line maps (Figs. 1*a* and 1*b*) is the morphology of the ionized gas seen to the northwest of the nucleus, which resembles a "figure eight," or two overlapping S-shaped emission-line strands. The southeast part of the NLR is markedly different: the NLR is much narrower close to the nucleus, extends at least twice as far from the nucleus as the northwest part, and toward the end splits into several strands of emission-line gas which turn toward the north. Despite these differences in detail, the emission-line gas on both sides of the nucleus is dominated by partially resolved strands which are only 10–20 pc wide but 100–300 pc long. Because they are so narrow, the strands are best seen on the Hα image (Fig. 1*a*), which has higher spatial resolution than the [O III] image.

Besides the strands, we find a few fainter structures in our emission-line images that are of potential interest. There is a faint arc of emission-line gas some 1″ (100 pc) south of the east end of the emission-line strands, best seen in the [O III] image. On the Hα image we notice two weak blobs 5″ to the southeast and 3″ to the south-southeast of the nucleus. On the other side of the NLR, a faint, linear emission-line feature extends from the "figure eight" to the northwest. It is ∼1.″1 long and points directly toward the nucleus. At the same distance (2.″2 from the nucleus) in the opposite direction, the emission from the lower part of the emission-line arc is also slightly enhanced.

Interestingly, these linear features to the northwest and southeast, the nucleus itself, and the 5″ southeast Hα blob align to within a few degrees. The odds for a chance alignment are minimal, given the fact that we see only two isolated Hα blobs within the central 10″ × 10″, and the question arises whether the blob 5″ southeast of the nucleus is excited or has been expelled by the nuclear source. We therefore smoothed the [O III] and Hα images with a 0.″2 beam to increase the signal-to-noise ratio, and determined the [O III]/Hα ratio for the blob and the linear features. While the linear features have [O III]/Hα $\gtrsim 2$, consistent with being excited by an AGN spectrum, the southeast blob has [O III]/Hα $\sim \frac{1}{3}$.

To learn more about the excitation, we have divided the [O III] image by the Hα image at the resolution of the WF pixels. In Figure 1*c*, regions of darker shades indicate higher [O III]/Hα ratios and hence regions of higher excitation. The excitation structure to the southeast of the nucleus and within 2″ of it bears some resemblance to the ionization cones seen in other Seyfert 2 galaxies. If one interprets this structure as being due to a cone of exciting radiation, the opening angle would be around 45°–50°. The structure on the other side of the nucleus is consistent with the presence of a similar, but shorter, cone. The average [O III]/Hα ratio along the central axis of the cone is around 2. There is, however, a noticeable trend for the excitation to decrease toward the northwest. This could be understood as a result of increased reddening in this direction.

Toward the southeast end of the nebulosity, in the region

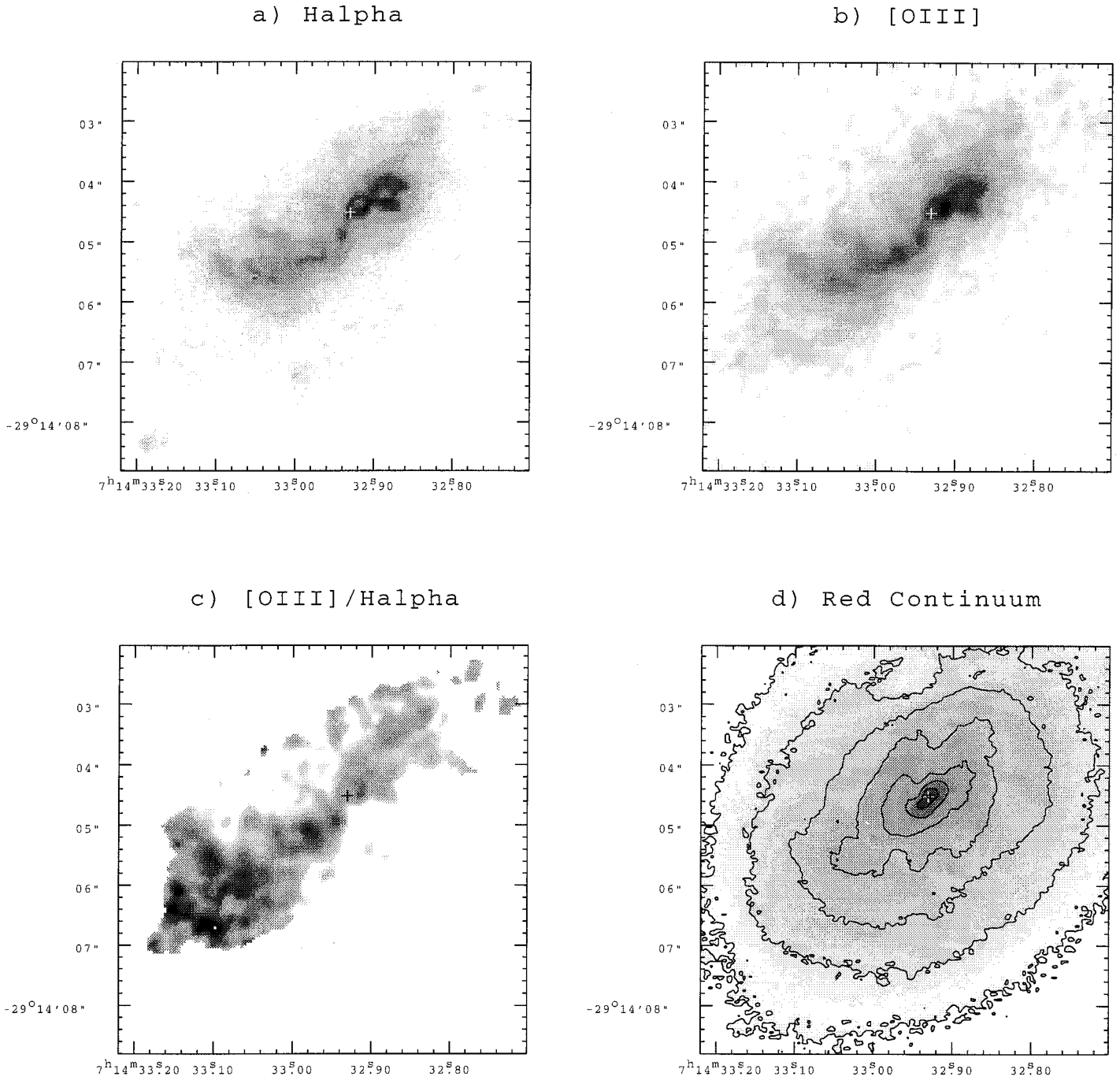


FIG. 1.—(*a*) Continuum-subtracted H$\alpha$ image of the narrow-line region of ESO 428-G14 taken with the Planetary Camera (0.″0544 resolution). The flux in the central $4'' \times 4''$ is $8.2 \times 10^{-13}$ ergs s$^{-1}$ cm$^{-2}$, and the intensity scale here and in the following is proportional to the square root of the brightness. The continuum peak of the galaxy is marked by a cross, and the B1950 coordinates are from the 6 cm radio map (see Fig. 2). (*b*) Continuum-subtracted [O III] image of the narrow-line region of ESO 428-G14 taken with the Wide Field Camera (0.″1 resolution). The flux in the central $4'' \times 4''$ is $1.5 \times 10^{-12}$ ergs s$^{-1}$ cm$^{-2}$. (*c*) Excitation map of ESO 428-G14, obtained by dividing [O III] by H$\alpha$. Dark shades represent regions of high excitation; the gray scale ranges from 1.2 to 4 for the [O III]/H$\alpha$ ratio. (*d*) Red continuum filter (F814W) image of the host galaxy overlaid with logarithmic isophotes (0.″0544 resolution).

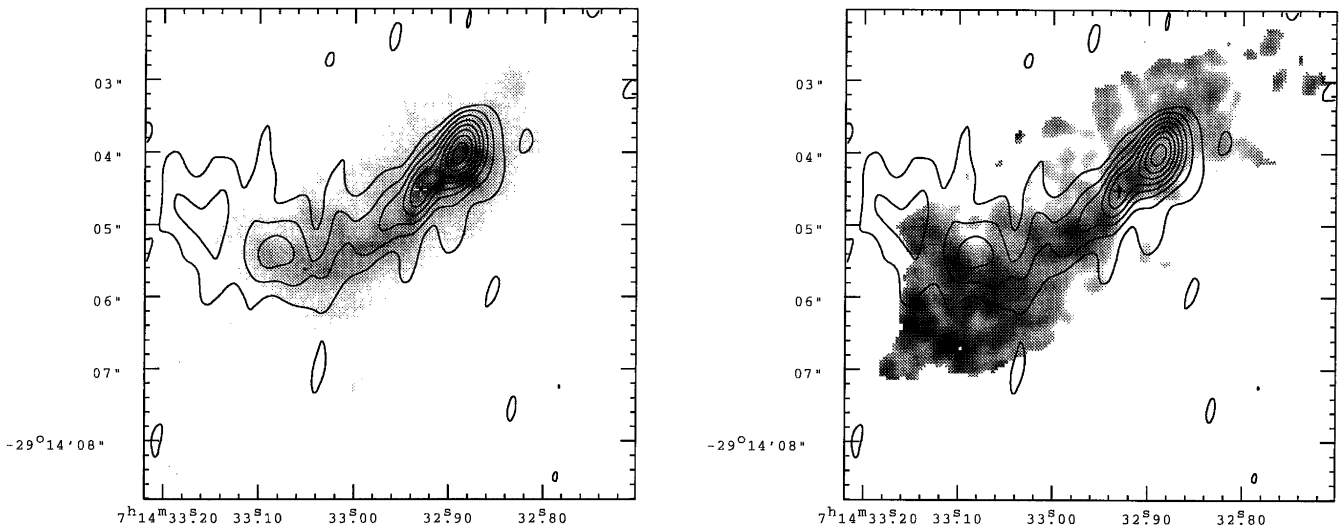


FIG. 2.—H$\alpha$ and excitation map (both with linear gray scale) of ESO 428-G14 as in Fig. 1, overlaid with the contours of the 6 cm map from Ulvestad & Wilson (1989), which has a beam of 0".3 × 0".6. The B1950 coordinate grid is also taken from this map. The uncertainties in the registration between the VLA and the *HST* maps are ~0".2.

where the radio jet and the last strand bend toward the north, the excitation in the gas is relatively high. The average [O III]/H$\alpha$ here is around 3.2. The faint arc to the south of the east end of the strands also has higher than average excitation, but here the data are noisy. The highest excitation found in this map—close to the nucleus—is around 3.5.

Finally, we present the red broadband image of the galaxy in Figure 1*d*. Within the inner 100 pc, a spiral feature extends from the nucleus to the southeast and then turns toward the north. The continuum nucleus is clearly elongated on a scale of a few tenths of an arcsecond along the direction of the NLR, and farther out the contours are disturbed at the position of the bright emission-line strands. The galaxy extends farther than the section shown in Figure 1*d*, but even on the full field of view we do not see any large-scale spiral arms.

### 3.2. *Comparison with Radio Map*

The absolute astrometric uncertainties for *HST* positions with respect to the radio reference frame are of the order of 1" and hence cannot be used to align the *HST* and the VLA maps of ESO 428-G14. However, we smoothed the *HST* image to the resolution of the radio map (0".3 × 0".6) and found that the smoothed emission-line image is very similar to the radio map. If we then make the reasonable assumption that the radio and optical structures should align, we can shift the optical map until the structures coincide. Even though the radio and optical emission are sometimes anticorrelated in detail (e.g., Mulchaey et al. 1994), the similarity of the radio continuum and optical emission-line structures of ESO 428-G14 suggests that this is not a major problem here.

However, within an accuracy of 0".2, the pixel-to-pixel registration for the two maps becomes rather arbitrary. To make a quantifiable registration, we have arbitrarily aligned the second brightest radio blob (some 0".75 southeast of the brightest radio feature) with the optical continuum peak. Figure 2*a* shows the contours of the radio map of Ulvestad & Wilson (1989) overlaid on the shifted H$\alpha$ image with this alignment. The B1950 coordinate grids on Figure 1 were also taken from the radio map. With this final alignment, the shifts between the *HST* and the VLA coordinate grids are 1".0 in right ascension and 0".4 in declination, and hence within the typical astrometric uncertainties of the *HST*.

Provided our registration is correct, the first result of this comparison is that the brightest peak of the radio emission is associated with the northwest part of the NLR (the "figure eight") and is displaced by ~0".75 from the optical continuum peak. We therefore conclude that the radio jet is indeed not one-sided, but rather two-sided and asymmetric, as speculated by WB89. Like the emission-line structure, the northwest side of the radio jet is very short and terminates in a bright hot spot, while there is no well-defined terminus to the southeast, where the radio jet and emission-line strands bend toward the north. However, the somewhat higher excitation seen in the [O III]/H$\alpha$ map (Fig. 2*b*) along the bent of the radio jet in the southeast may indicate some increased jet/interstellar medium (ISM) interaction.

The only structure which does not have a correspondence in the radio map is the emission-line arc to the south of the southeast tip of the NLR. Because of the lower resolution of the radio map and the uncertainty of registration, we also cannot tell whether the emission-line strands themselves are associated with radio-emitting plasma.

## 4. DISCUSSION

In general ESO 428-G14 fits quite nicely into the basic picture we have for Seyfert 2 galaxies within the unified scheme. The ionization structure as seen in the excitation map is highly elongated and consistent with a faint bicone, even though the structure is less convincing than in the best cases of "ionization cones" (e.g., Tadhunter & Tsvetanov (1989). We also confirm the results of WB89 that the emission-line gas is elongated in the same direction as the radio outflow, which seems to be a general feature of Seyfert galaxies.

The most remarkable result for ESO 428-G14, however, is the shape of the NLR and its close correspondence to the radio jet, which allowed us to align radio and optical maps fairly accurately. The emission from the NLR of ESO 428-G14 is dominated by well-ordered strands of emission-line gas which are some 10 pc thick, but can be more than 100 pc long. In the northwest part of the jet, we find two strands organized

in a "figure eight" shape that is very suggestive of a double helix. This may indicate that the emission-line strands are produced at the surface of the radio jet, possibly by an interaction of the jet with the ISM. Helical structures associated with radio jets seem to be quite common: some VLBI components of quasar jets seem to move on helical trajectories (see, e.g., Steffen et al. 1995), and Cecil, Wilson, & Tully (1992) demonstrated that the H$\alpha$ jet in NGC 4258 consists of helically twisted strands in a triple helix.

The comparison with NGC 4258 is even more striking if one considers the region to the southeast, where the jet tapers off. The strands in NGC 4258 become detached from each other, leave the helical structure, and end up pointing in different directions. This is similar to the southeast part of the ESO 428-G14 jet, where the relatively narrow emission-line structure splits into various strongly bent fingers. Moreover, in both galaxies, the untwisting of the strands happens at the end of the jet and is associated with strong jet bending. This similarity may suggest that even if we cannot resolve the well-collimated structure just to the southeast of the nucleus of ESO 428-G14, there may well be a tightly twisted string of helical strands, as in NGC 4258. On the other hand, it is striking that the helices on opposite sides of the nucleus of ESO 428-G14 should have such very different pitch angles. It may therefore be that we see only one strand of a wide helix in the southern jet, which then splits into multiple strings.

What processes can be responsible for these helical strands in ESO 428-G14? The only plausible place to produce such strands is the boundary layer between the radio jet and the ISM. In NGC 4258, it has been argued that the jet creates a low-density tunnel through the ISM (Martin et al. 1989). A similar process may occur in ESO 428-G14. Interactions between the jet and the denser ISM could then induce fluid instabilities and entrainment in the jet; the pros and cons of these models are discussed extensively in Cecil et al. (1992).

Another question that immediately comes to mind when looking at Figure 1*a* is whether the optical emission-line strands could be associated with strong magnetic field lines. Those field lines would have to be frozen into the plasma on the surface of the jet, which is ionized by the central source (the fact that the strands do not show up in the excitation map suggests that there is little or no local ionization). Such prominent, large-scale magnetic field lines do indeed exist, as seen, for example, in the Galactic center nonthermal filaments (Yusef-Zadeh & Morris 1987) or in other exotic radio sources (e.g., Gray 1996).

In any case, it appears from our images that the morphology of the NLR is largely governed by the bipolar outflow. WB89 have found that the emission lines in ESO 428-G14 have extended red wings to the northwest of the nucleus, and extended blue wings to the southeast, with speeds up to 1400 km s$^{-1}$. This suggests that the northwest jet is moving away from us and the southeast jet toward us. Such an orientation would be consistent with the apparently larger reddening to the northwest that we inferred from the lower [O III]/H$\alpha$ ratio in the northwest (§ 3.1).

Besides the strands, we find other signs of the interaction between the jet and the ISM. As mentioned before, along the large-scale bend of the southeast jet we find a ridge of enhanced excitation. An association between jet terminus and enhanced [O III] emission has also been found in many radio galaxies (McCarthy, Spinrad, & van Breugel 1995). The faint arc of emission-line gas we see beyond this ridge is reminiscent of the spectacular arcs found in the Seyfert galaxy Mrk 573 (Capetti et al. 1996), where the arcs were interpreted as shock fronts. However, in ESO 428-G14 the jet does not even seem to reach this arc, and deeper radio maps are needed to investigate this phenomenon in more detail.

Finally, we consider the two faint, linear features that are symmetrically placed in opposite directions 2.″2 from the nucleus: the northwest feature is well visible in Figure 1*a*, while the southeast feature is on top of the faint arc and less apparent. The presence of these features is suggestive of a highly collimated beam of ionizing photons escaping from the center. In NGC 3516 a similar feature pointing toward the nucleus was seen by Miyaji, Pérez-Fournon, & Wilson (1992) and cautiously interpreted as ambient gas illuminated by UV radiation from a relativistic jet. The low-excitation blob with cometary-like tail 5″ southeast of the nucleus is aligned in the same directions, but in view of its low excitation this blob might be just an H II region.

Despite the many open questions, ESO 428-G14 may contribute significantly to our understanding of the NLR of AGNs and the jet/ISM interaction. The galaxy shows the main features seen in various Seyfert and radio galaxies, i.e., a possible ionization cone and a close association between radio synchrotron and optical emission-line gases. It also demonstrates that the structure of the NLR cannot be understood without considering the influence of the jet on the ISM. Higher resolution radio maps are needed to determine whether the strands of ionized gas are also sources of enhanced synchrotron emission.

This research was supported by NASA under grants NAGW-3268 and NAG8-1027. We thank the STScI staff—especially J. Biretta, M. McMaster, and K. Rudloff—for their support in the LRF calibrations, and an anonymous referee for helpful remarks.

REFERENCES

Antonucci, R. 1993, ARA&A, 31, 473
Baum, S. A., & Heckman, T. 1989, ApJ, 336, 702
Bergvall, N., Johansson, L., & Olofsson, K. 1986, A&A, 166, 92
Boksenberg, A., et al. 1995, ApJ, 440, 151
Bower, G. A., Wilson, A. S., Mulchaey, J. S., Miley, G. K., Heckman, T. M., & Krolik, J. H. 1994, AJ, 107, 1686
Capetti, A., Axon, D. J., Macchetto, F., Sparks, W. B., & Boksenberg, A. 1996, ApJ, 469, 554
Cecil, G., Wilson, A. S., & Tully, R. B. 1992, ApJ, 390, 365
de Bruyn, A. G., & Wilson, A. S. 1978, A&A, 64, 433
de Vaucouleurs, G., de Vaucouleurs, A., Corwin, H. G., Buta, R. J., Paturel, G., & Fouqué, P. 1992, Third Reference Catalogue of Bright Galaxies (New York: Springer)
Falcke, H., Malkan, M., & Biermann, P. L. 1995, A&A, 298, 375
Gray, A. 1996, in ASP Conf. Ser., The Galactic Center, ed. R. Gredel (San Francisco: ASP), in press
Haniff, C. A., Wilson, A. S., & Ward, M. J. 1988, ApJ, 334, 104
Martin, P., Roy, J.-R., Noreau, L., & Lo, K. Y. 1989, ApJ, 345, 707
McCarthy, P. J., Spinrad, H., & van Breugel, W. 1995, ApJS, 99, 27
Miyaji, T., Wilson, A. S., & Pérez-Fournon, I. 1992, ApJ, 385, 137
Mulchaey, J. S., & Wilson, A. S. 1995, ApJ, 455, L17
Mulchaey, J. S., & Wilson, A. S., Bower, G. A., Heckman, T. M., Krolik, J. H., Miley, G. K. & 1994, ApJ, 433, 625
Pogge, R. W. 1988, ApJ, 332, 702
Rawlings, S., Saunders, R., Eales, S. A., & Mackay, C. D. 1989, MNRAS, 240, 701
Steffen, W., Zensus, J. A., Krichbaum, T. P., Witzel, A., & Qian, S. J. 1995, A&A, 302, 335
Tadhunter, C., & Tsvetanov, Z. 1989, Nature, 341, 422
Ulvestad, J. S., & Wilson, A. S. 1989, ApJ, 343, 659
Unger, S. W., Pedlar, A., Axon, D., Whittle, M., & Meurs, E. J. A. 1987, MNRAS, 228, 671
Wilson, A. S., & Baldwin, J. A. 1989, AJ, 98, 2056 (WB89)
Wilson, A. S., Braatz, J. A., Heckman, T. M., Krolik, J. H., & Miley, G. K. 1993, ApJ, 416, L61
Yusef-Zadeh, F., & Morris, M. 1987, ApJ, 322, 721